Evaluation of a New Ultrasound Thoracoscope for Localization of Lung Nodules in Ex Vivo Human Lungs

Hideki Ujiie, MD, PhD, Tatsuya Kato, MD, PhD, Hsin-pei Hu, MHS, Suhaib Hasan, Priya Patel, MD, Hironobu Wada, MD, PhD, Daiyoon Lee, MS, Kosuke Fujino, MD, PhD, David M. Hwang, MD, PhD, Marcelo Cypel, MD, MS, Marc de Perrot, MD, MS, Andrew Pierre, MD, MS, Gail Darling, MD, Thomas K. Waddell, MD, PhD, Shaf Keshavjee, MD, MS, and Kazuhiro Yasufuku, MD, PhD

Division of Thoracic Surgery, Toronto General Hospital, and Department of Pathology, University Health Network, University of Toronto, Toronto, Ontario, Canada

Background. **Localization of small, nonvisible and nonpalpable nodules is challenging during video-assisted thoracoscopic surgery. We evaluated the feasibility of using a new ultrasound thoracoscope to localize nodules in resected ex vivo human lungs.**

Methods. **The tumor was localized and measured in its greatest dimension with a prototype ultrasound thoracoscope (XLTF-UC180; Olympus Corporation, Tokyo, Japan) at different frequencies (5.0 to 12.0 MHz) and different lung specimen states (deflated, semiinflated). Measured tumor size and depth from lung surface were compared and correlated to the true diameter and depth from lung surface acquired from pathologic morphology.**

Results. **Ex vivo evaluation was performed on 16 solid nodules and nine part solid ground-glass nodules. All tumors were successfully localized in the deflated lung specimens (average size, 13.7 ± 5.2 mm). The tumor boundaries were best evaluated with an ultrasound frequency of 10 MHz. Solid nodules were more easily visualized than ground-glass nodules. Part solid ground-glass nodules were not easily detected in the semiinflated specimen owing to peritumoral air surrounding the tumor. Tumor boundaries were also difficult to identify in deeply situated tumors and in lungs with underlying disease. A strong positive correlation existed between the ultrasound measurement and true measurement of tumor size ($R^2 = 0.89$, $p < 0.001$).**

Conclusions. **The ultrasound thoracoscope can be used to localize nodules in resected human lungs. The clarity of the tumor boundaries is influenced by the tumor type and depth and the underlying pulmonary disease. Complete lung deflation and the use of 10 MHz ultrasound frequency optimize the visualization of target tumors.**

(Ann Thorac Surg 2017;103:926–34)

The results of the National Lung Screening Trial showing that low-dose computed tomography (CT) screening reduces lung cancer mortality have led to the adoption of lung cancer screening in centers around the world [1]. Thoracic surgeons are now frequently being asked to manage patients with small pulmonary nodules. Video-assisted thoracoscopic surgery (VATS) has become the standard of care for patients with early stage lung cancer. In particular, VATS wedge resection is widely used in patients with small peripheral pulmonary nodules, including metastatic tumors and indeterminate lesions. However, one of the clinical challenges during VATS wedge resection is real-time precise localization of the tumor, especially for small, nonvisible and nonpalpable lesions. Failure to localize lesions may result in larger resections or conversion to thoracotomy.

Preoperative CT-guided metal tag placement (eg, a microcoil or a hook wire) with intraoperative fluoroscopic assistance has become the prevalent method of localizing small pulmonary nodules, and has been highly successful in localizing nodules, with success rates greater than 97% [2, 3]. However, the metal tag placement procedure requires a preoperative invasive procedure that can result in patient discomfort. Complications such as metal tag dislodgement, pneumothorax, and hemoptysis may also occur. Furthermore, use of CT makes intraoperative radiation exposure inevitable for both patients as well as operating staff.

Accepted for publication Aug 8, 2016.

Presented at the Sixteenth Annual Meeting of the International Society for Minimally Invasive Cardiothoracic Surgery, Montreal, Quebec, Canada, June 15–18, 2016.

Address correspondence to Dr Yasufuku, Division of Thoracic Surgery, Toronto General Hospital, 200 Elizabeth St, 9N-957, Toronto, ON M5G2C4, Canada; email: kazuhiro.yasufuku@uhn.ca.

Dr Yasufuku discloses a financial relationship with Olympus Corporation.

0003-4975/$36.00
http://dx.doi.org/10.1016/j.athoracsur.2016.08.031

Thoracoscopic ultrasonography is a compelling alternative to CT-guided nodule localization as it offers minimally invasive, real-time localization without any preoperative procedures and their associated risks. The procedure is also cheaper and less time consuming. Previous small-scale, single-center studies have demonstrated the feasibility of intraoperative ultrasonography for localization of small lung nodules [4–12], including ground-glass nodules (GGN) [5]. However, the use of ultrasonography in thoracic surgery is limited, likely because of the lack of commercial probes designed for thoracic surgery. The closest available alternatives, abdominal probes, have difficulty accessing certain areas of the lung owing to their structures.

Consequently, we have been developing an ultrasound thoracoscope that enables precise visualization and real-time biopsy of small lung nodules during VATS. Our previous initial study, which tested the prototype ultrasound thoracoscope in animal tumor models, yielded positive results as the use of the ultrasound thoracoscope resulted in a nodule detection rate of 93.3% at depths as great as 24.8 mm [13]. The aim of this study was to assess the effectiveness of the ultrasound thoracoscope in resected human lungs and to explore optimal ultrasound settings for intraoperative lung nodule localization before initiating a human clinical trial.

Patients and Methods

Ultrasound Thoracoscope

This clinical study was approved by the Institutional Review Board at University Health Network, and all patients gave informed consent (protocol number: 13-7111). All data collection and analysis pertaining to the study were performed at University Health Network. A newly developed prototype ultrasound thoracoscope (XLTF-UC180; Olympus Corporation, Tokyo, Japan) was used for this study (Fig 1) [13]. This semirigid ultrasound thoracoscope has a tip capable of flexing up and down, and a convex ultrasound probe that is situated at the tip. The operating frequencies of the ultrasound thoracoscope are 5, 7.5, 10, and 12 MHz; and its scanning range is 60 degrees. The outer diameter is 10 mm for the use of minimally invasive surgery. A charge-coupled device camera and two light sources are on the tip of the thoracoscope. The accessory channel diameter is 2.2 mm. A dedicated 22G needle can be used to obtain tissue samples. Images obtained using this ultrasound thoracoscope can be recorded in an ultrasound scanner (EU-Y0005; Olympus Corporation) to be used for data analysis.

Participants

In this single-institution clinical trial, 25 participants aged 18 years or older were enrolled. Participants were scheduled to undergo malignant lung tumor resection through VATS lobectomy or segmentectomy. Patients were excluded from the study if they were having multiple nodules resected.

Ultrasound Thoracoscope Evaluation

After surgery, the resected specimen was placed on a surgical table in an ex vivo setting mimicking the actual position of the lung in vivo. The resected ex vivo lungs were used to evaluate the ultrasound thoracoscope (Fig 1C). The dimensions of the tumor were obtained using the ultrasound thoracoscope for the specimen in the deflated state. After evaluation in the deflated state, a 19G needle catheter was inserted to bronchial stump. The resected specimen was semiinflated with air pushed through a syringe attached to the inserted catheter. No acoustic coupling agent such as ultrasound gel was used for visualizing the structure. Different ultrasound frequencies (5, 7.5, 10, and 12 MHz) were used while measuring the tumor size. After ultrasound evaluation, sections of the specimen were evaluated for size and depth of the tumor. After evaluation by ultrasound, the lung tumor was sectioned on the nearest lung surface. We measured tumor size and distance from the lung surface to the tumor and distal boundary on sections of the specimen. Ultrasound measurements of the tumor size and the depth were compared and correlated to the true measurements. Histologic diagnoses of tumors were made based on the fourth edition of the World Health Organization classification [14, 15].

Statistical Analysis

The Mann-Whitney *U* test was used to compare continuous variables such as tumor size and tumor depth from the lung surface. A two-by-two contingency table was created for Fisher's exact test to compare the distinctness of tumor borders. The square of the Pearson correlation coefficient (R^2) was computed between the actual tumor diameter, the tumor diameter on CT imaging, and the tumor diameter on ultrasound imaging. Statistical analyses were conducted using R (version 3.0.1; R Foundation for Statistical Computing, Vienna, Austria). All p values were based on a two-sided hypothesis, and a p value of less than 0.05 was considered to have statistical significance.

Results

The demographic information is given in Table 1. Of the 25 cases, 19 (76%) were lobectomy cases and 6 (24%) were segmentectomy cases. The average tumor size on preoperative CT image was 16.8 $\pm$ 4.5 mm (range, 8 to 27.2 mm). The depth of the tumor from lung surface was 10.1 $\pm$ 8.8 mm on average (range, 0 to 30 mm), and the deepest visualized tumor boundary was 28.6 $\pm$ 7.8 mm on average (range, 19 to 47 mm). Based on consolidation to tumor ratio of CT images, 16 cases (64%) were categorized as solid nodules, which are more than 50% consolidation to tumor ratio; and 9 cases (36%) were categorized as part solid GGNs, which are less than 50% consolidation to tumor ratio. On final diagnosis, 14 cases (56%) were invasive adenocarcinoma, 4 (16%) were metastatic lung tumors (1 leiomyosarcoma, 1 pancreatic cancer, 2 endometrial carcinoma), 3 (12%) were squamous cell

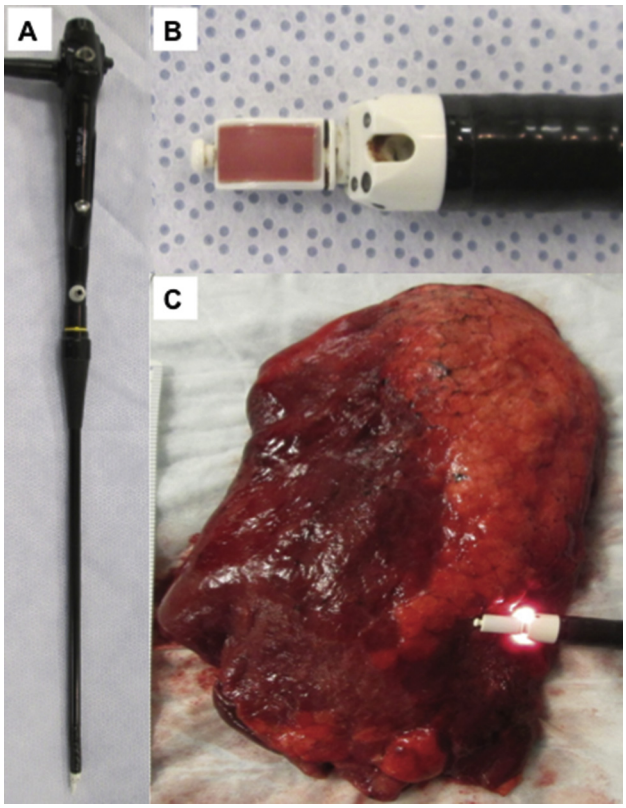

Fig 1. (A) Body of the prototype ultrasound thoracoscope (XLTF-UC180; Olympus, Tokyo, Japan). (B) Tip of the ultrasound thoracoscope. The outer diameter is 10 mm for use in minimally invasive surgery. A charge-coupled device camera and two light sources are situated on the tip of the thoracoscope. The accessory channel diameter is 2.2 mm. (C) The ultrasound thoracoscope is placed on the deflated human lung surface to localize lung tumors.

carcinoma, 2 (8%) were typical carcinoid, 1 (4%) was atypical carcinoid, and 1 (4%) was a solitary fibrous tumor. Of the 14 invasive adenocarcinoma cases, 2 (14%) were lepidic predominant, 7 (50%) were acinar predominant, 2 (14%) were papillary predominant, and 3 (22%) were solid predominant adenocarcinomas [15].

With the specimen in the deflated state, all 25 tumors were successfully visualized with the ultrasound thoracoscope (sensitivity 100%: detected = 25, evaluated = 25; Fig 2). The average tumor size on ultrasound was 13.7 ± 5.2 mm (range, 4.1 to 26.1 mm). The depth from lung surface to tumor on ultrasound image was 1.1 ± 0.9 mm on average (range, 0 to 3.4 mm), and the deepest visualized tumor boundary was 14.8 ± 5.1 mm (range, 5.7 to 26 mm). Tumor margins of part solid GGNs were less clear compared with the margins of solid nodules in both the deflated and inflated state. In the deflated state, ultrasound visualized the deepest tumor margins of all nodules. However, in the semiinflated state, the deepest tumor margins for four partly solid GGNs were difficult to visualize owing to residual air (Fig 3).

Each tumor was visualized using four different ultrasound frequencies (5, 7.5, 10, and 12 MHz). That was done to determine optimal settings for the ultrasound thoracoscope. Based on the review of the ultrasound images by thoracic surgeons (H.U. and T.K.), higher frequencies provided clearer tumor images for the 5 to 10 MHz range. When comparing images produced by frequencies of 12 MHz and 10 MHz, it appeared that 12 MHz was better for visualizing shallower tumors whereas 10 MHz was better for visualizing deeper tumors (Fig 2). We compared the ultrasound and pathologic images of each adenocarcinoma morphologic subtype (Fig 4). All of the ultrasound images showed clear margins in the deflated state. Ultrasound images corresponded with the microscopic images.

With the specimen in the inflated state, the average pathologic tumor size for the 25 evaluated tumors was 15.5 ± 6.8 mm (range, 5 to 32 mm). The distance from lung surface to tumor were 3.6 ± 5.3 mm on average (range, 0 to 20 mm), and the deepest visualized tumor boundary was 19.7 ± 9.5 mm on average (range, 7.9 to 52 mm). Two (8%) of the 25 tumors showed indistinct tumor margins. These cases were GGNs, and one other tumor was situated in an emphysematous lung. The indistinctiveness of tumors was also associated with tumor depth as tumors located in a deeper part of the lung were more challenging to visualize. The comparison of actual tumor size and ultrasound tumor size showed statistically significant and stronger correlation ($R^2 = 0.89$, $p < 0.001$) than the actual tumor size compared with the CT tumor size ($R^2 = 0.67$, $p < 0.001$; Fig 5).

Next, we compared the image quality of the ultrasound thoracoscope with a commercially available laparoscopic ultrasound device (8666-RF; BK Medical, Peabody, MA) as shown in Figure 6. In the 10 cases evaluated, tumor margins were identified more clearly in the images acquired from the ultrasound thoracoscope than from the laparoscopic ultrasound device. The laparoscopic ultrasound probe is bigger than the ultrasound thoracoscope probe; therefore, it was almost impossible to achieve complete contact of the probe with the lung surface at any given point in time. Moreover, although visible using the ultrasound thoracoscope, GGNs were nearly impossible to visualize when using the laparoscopic ultrasound device (data not shown).

Comment

Despite its successful implementation in various surgical disciplines, intraoperative ultrasonography has yet to establish a significant role in thoracic surgery. Nonetheless, a number of studies have shown that thoracoscopic ultrasonography may be a viable method for visualizing pulmonary nodules during VATS. When compared with more conventional methods of nodule localization during VATS, thoracoscopic ultrasonography has several advantages [4–12]. It provides real-time localization of nonpalpable nodules, does not require any invasive preoperative procedures, and potential risks of complications such as pneumothorax and hemoptysis are avoided [7]. Furthermore, the procedure can potentially be done at a low cost as it does not require any additional

Table 1. Characteristics of Lung Tumors

			Computed Tomography Imaging					Ultrasound Imaging Deflated Lung		Pathology Findings		
Case	Location	Procedure	Nodule Finding	Tumor Size (mm)	Consolidation Tumor Size (mm)	C/T Ratio (%)	Depth[a] (mm)	Tumor Size (mm)	Depth[a] (mm)	Diagnosis	Tumor Size (mm)	Depth[a] (mm)
1	RLL	Lobectomy	PS GGN	14.5	7	48	6.5	10.1	1	Adenocarcinoma (PAP)	13	1
2	LLL	Segmentectomy	SN	11	11	100	12.4	11.3	1.3	Metastatic lung tumor	11	1.5
3	RLL	Lobectomy	SN	17.6	17.6	100	27.6	10.7	2.1	Typical carcinoid	13	4
4	RML	Lobectomy	SN	14.9	13.8	93	11.8	12.7	1.7	Metastatic lung tumor	13	1.2
5	LUL	Lobectomy	PS GGN	13	6	46	8.3	7.7	1	Adenocarcinoma (ACI)	10	1
6	LUL	Segmentectomy	PS GGN	18	9	50	0	11.7	0	Adenocarcinoma (LEP)	18	0
7	LLL	Lobectomy	SN	8	6.8	85	15.3	4.1	1.6	Adenocarcinoma (SOL)	5	2.9
8	RML	Lobectomy	SN	17	16	94	30	11.6	1.4	Metastatic lung tumor	15	3
9	RML	Lobectomy	SN	27.2	26.8	99	0	26.1	1.1	Adenocarcinoma (SOL)	30	1
10	RLL	Segmentectomy	SN	16.3	15	92	0	13.3	0	Metastatic lung tumor	17	0
11	RUL	Lobectomy	PS GGN	22	10	45	4.3	10.4	2	Adenocarcinoma (ACI)	13	1
12	LLL	Segmentectomy	SN	21.9	18.4	84	11.6	10.5	3.4	Typical carcinoid	21	5
13	RUL	Lobectomy	PS GGN	16.1	8	50	0	14.4	0	Adenocarcinoma (ACI)	15	0
14	LUL	Segmentectomy	PS GGN	17	6.2	36	0	11.2	0	Adenocarcinoma (LEP)	13	0
15	RLL	Lobectomy	PS GGN	22	10	45	19.5	25	1	Adenocarcinoma (ACI)	32	20
16	LUL	Lobectomy	PS GGN	16.8	8	49	20.2	13	1	Adenocarcinoma (ACI)	13	18
17	RUL	Segmentectomy	SN	17.3	16.8	97	10.1	14.2	3	Solitary fibrous tumor	15	10
18	RML	Lobectomy	SN	16.4	10.2	62	20.1	13.1	1	Adenocarcinoma (ACI)	13	2
19	LLL	Lobectomy	SN	19	19	100	0	21.4	0	Adenocarcinoma (SOL)	21	0
20	RML	Lobectomy	SN	13	11.4	88	4.4	10.2	1	Squamous cell carcinoma	12	1
21	RLL	Lobectomy	PS GGN	17	8	47	12.5	14	1	Adenocarcinoma (PAP)	12	1
22	RUL	Lobectomy	SN	18.5	10	54	0	12.5	0	Squamous cell carcinoma	12.5	0
23	LUL	Lobectomy	SN	11.2	11	98	13.4	24.4	1	Adenocarcinoma (ACI)	26	8
24	LUL	Lobectomy	SN	25	24	96	5	17.6	1	Squamous cell carcinoma	25	1
25	LUL	Lobectomy	SN	9	9	100	19	12.1	1.1	Atypical carcinoid	10	8

[a] Depth from lung surface to tumor.

ACI = acinar predominant; C/T = consolidation/tumor; GGN = ground-glass nodule; LEP = lepidic predominant; LLL = left lower lobe; LUL = left upper lobe; PAP = papillary predominant; PS = part solid; RLL = right lower lobe; RML = right middle lobe; RUL = right upper lobe; SN = solid nodule; SOL = solid predominant.

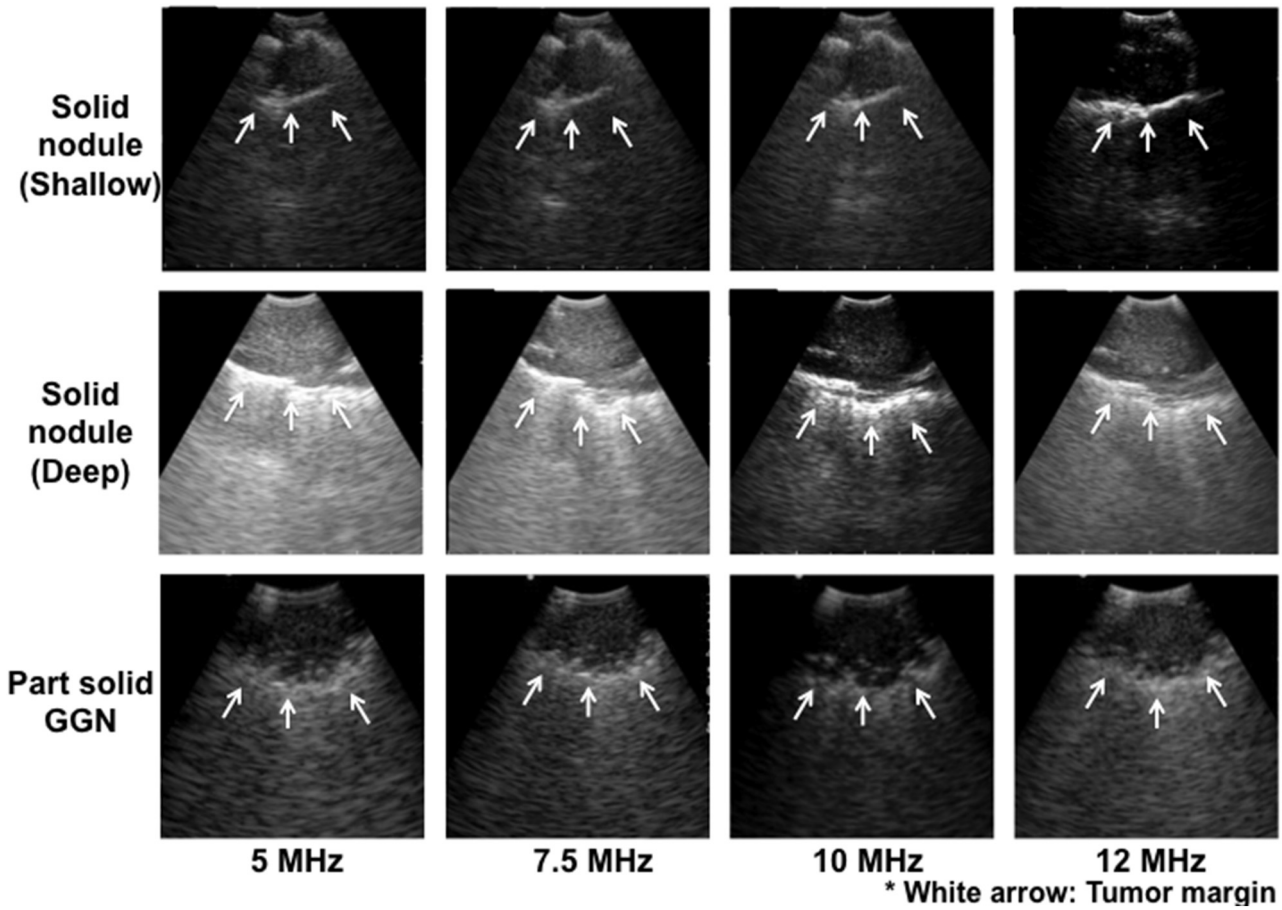

Fig 2. Comparison of lung adenocarcinoma scanned at the different frequencies in lung specimens (deflated state), with tumor margin visualization at 5 MHz, 7.5 MHz, and 10 MHz, respectively. Higher frequencies produced clearer images. Shallower tumor margins (top) are better visualized at 12 MHz whereas deeper tumor margins (bottom) are better visualized at 10 MHz. White arrows indicate tumor margin. (GGN = ground-glass nodule.)

preoperative procedure. Another advantage is that ultrasound technology provides access to most of the pleural surface during VATS, including the surface of complete fissures, which may be a challenge for finger palpation as well as for preoperative CT-guided metal tag placement. The current study aimed to evaluate a newly developed ultrasound thoracoscope—previously evaluated in animal models [13]—in resected human lung specimens.

On testing the ultrasound thoracoscope in 25 resected specimens, we found that the overall success rate of localizing small lung nodules was 100%. This number is in line with the success rate reported by previous studies (72.3% to 100%) [13]. The deepest visualized distal tumor boundary in ultrasound imaging was 26 mm from the lung surface. For a small lung nodule on CT imaging, 2 cases measuring less than 10 mm located more than 15 mm deep were successfully visualized. However, it is noteworthy that the clarity of the ultrasound image varied depending on a number of factors. The distance of the tumor from the lung surface had a significant influence on tumor visualization, as deeper tumors exhibited indistinct margins and were tougher to visualize. Whereas solid nodules were visualized with relative ease, visualization of part solid GGNs was more difficult. For instance, lepidic predominant adenocarcinoma was difficult to visualize through both ultrasound and CT imaging in the present study. It is likely that this difficulty in visualizing deeper and less solid tumors was due to residual air surrounding the tumors. Support for this idea is provided by the observation that pressing the ultrasound thoracoscope on the tumor's surface so as to push away some of the peritumoral residual air resulted in improved tumor visualization. When the lung's elasticity is compromised, as for the one emphysematous specimen in the present study, the increase in residual lung volume resulted in poor visualization of tumor margins. Although sufficient lung deflation may not always be possible, deflating the lung before ultrasound visualization is always preferred as it considerably improves visualization of deeper nodules and GGNs during surgery [5].

The available frequencies for current ultrasonography mainly range from 4 to 10 MHz. Some of the existing

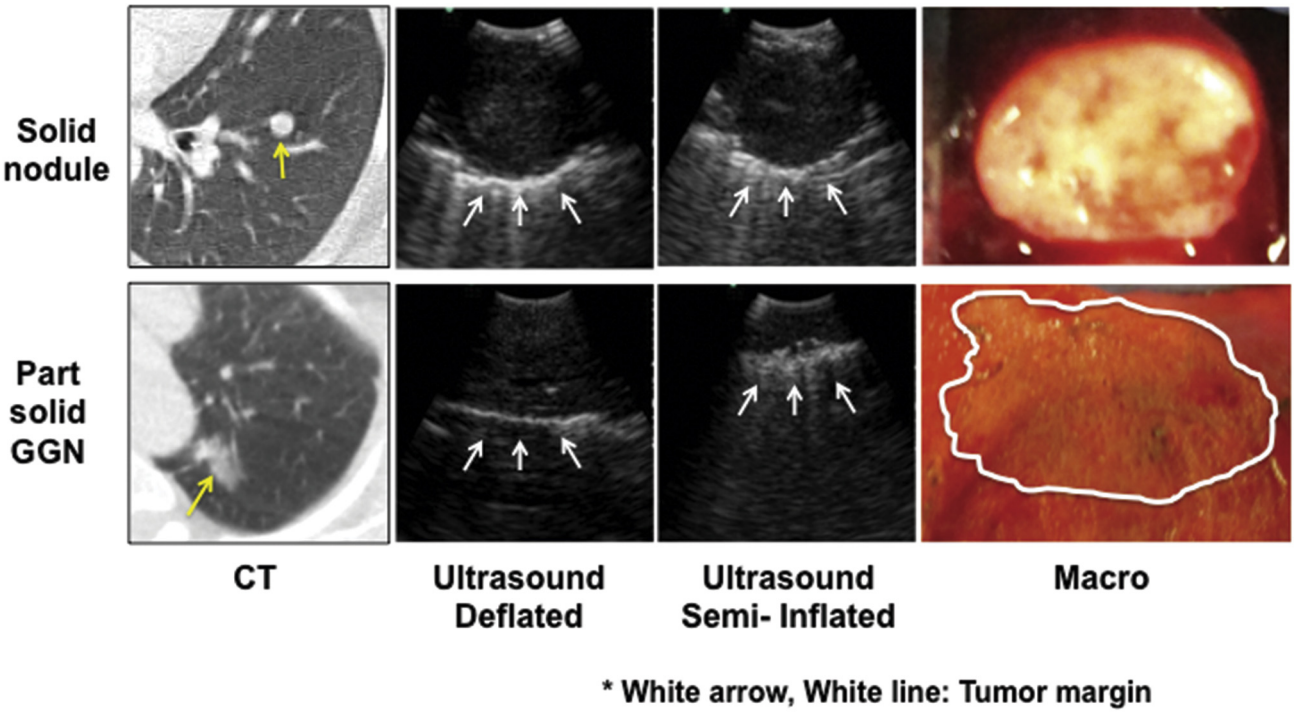

Fig 3. Comparison of computed tomography (CT), ultrasonography, and macroscopic (Macro) images between solid nodule and part solid ground-glass nodules (GGN) in both deflated and semiinflated states. Tumor margins are easier to visualize in the deflated state (left) compared with when the lung is semiinflated (right). On CT images, yellow arrows indicate tumor. On ultrasound images, white arrows indicate deepest border of lung tumor. On macroscopic image, white line marks entire tumor margin.

literature describes the use of higher frequencies. Ground-glass nodules can be detected by ultrasound at 7.5 MHz or 18 MHz [5]. In our experience, the frequency used to view the tumor also significantly affected image quality. Using 5, 7.5, and 10 MHz, tumor visualization was clearer at the highest frequency. That is in keeping with the idea that higher frequencies produce clearer images. However, when evaluating the image quality at 10 MHz and 12 MHz, the trend of the higher frequency producing the better image did not hold. In our experience, 12 MHz was the optimal frequency for tumor margins as deep as 15 mm. However, for tumors deeper than 15 mm, 10 MHz was the optimal frequency. An explanation for these observations is that the depth of penetration of the ultrasound beam is inversely proportional to the ultrasound frequency. With regard to our study, at 12 MHz the ultrasound beams would not have penetrated deep tumors as well as they would have at 10 MHz, resulting in a less clear tumor visualization. Conversely, with shallower tumors (depth to 15 mm), setting the ultrasound frequency at 12 MHz produced the clearer image, and perhaps a higher frequency would have produced even clearer images in this range.

In contrast to currently available probes, the ultrasound thoracoscope evaluated in the present study, designed specifically for thoracic surgery, has a number of important advantages. When we compared the ultrasound thoracoscope with the laparoscopic ultrasound device (8666-RF), commonly used in laparoscopic surgery, the visualization results suggested that the ultrasound thoracoscope is far superior. The laparoscopic ultrasound probe's rigid linear design makes it difficult to navigate the lung's surface and certain regions are unreachable. This limitation compromised the quality of the ultrasound image. The ultrasound thoracoscope, which has a greater scanning range owing to its flexible tip, is able to properly access and visualize more areas, ultimately increasing the probability of successfully localizing nodules during surgery. The laparoscopic ultrasound probe's larger size also becomes disadvantageous when scanning the lung, as it is nearly impossible for the entire probe to make contact with the lung at any given point. Meanwhile, the same difficulty is not had when scanning the lung using the ultrasound thoracoscope. The ultrasound thoracoscope's smaller probe size increases the likelihood of the entire probe making contact with the lung surface. The presence of residual air also seemed to have a greater impact on image quality in the laparoscopic ultrasound probe than it did in the ultrasound thoracoscope probe as the average difference between the inflated and deflated tumor margins was markedly higher. In addition, although visible using the ultrasound thoracoscope, GGNs were nearly impossible to visualize when using the laparoscopic ultrasound device. Nonetheless, it must be emphasized that when visualizing tumors, sufficient lung deflation is of great importance for both ultrasound devices.

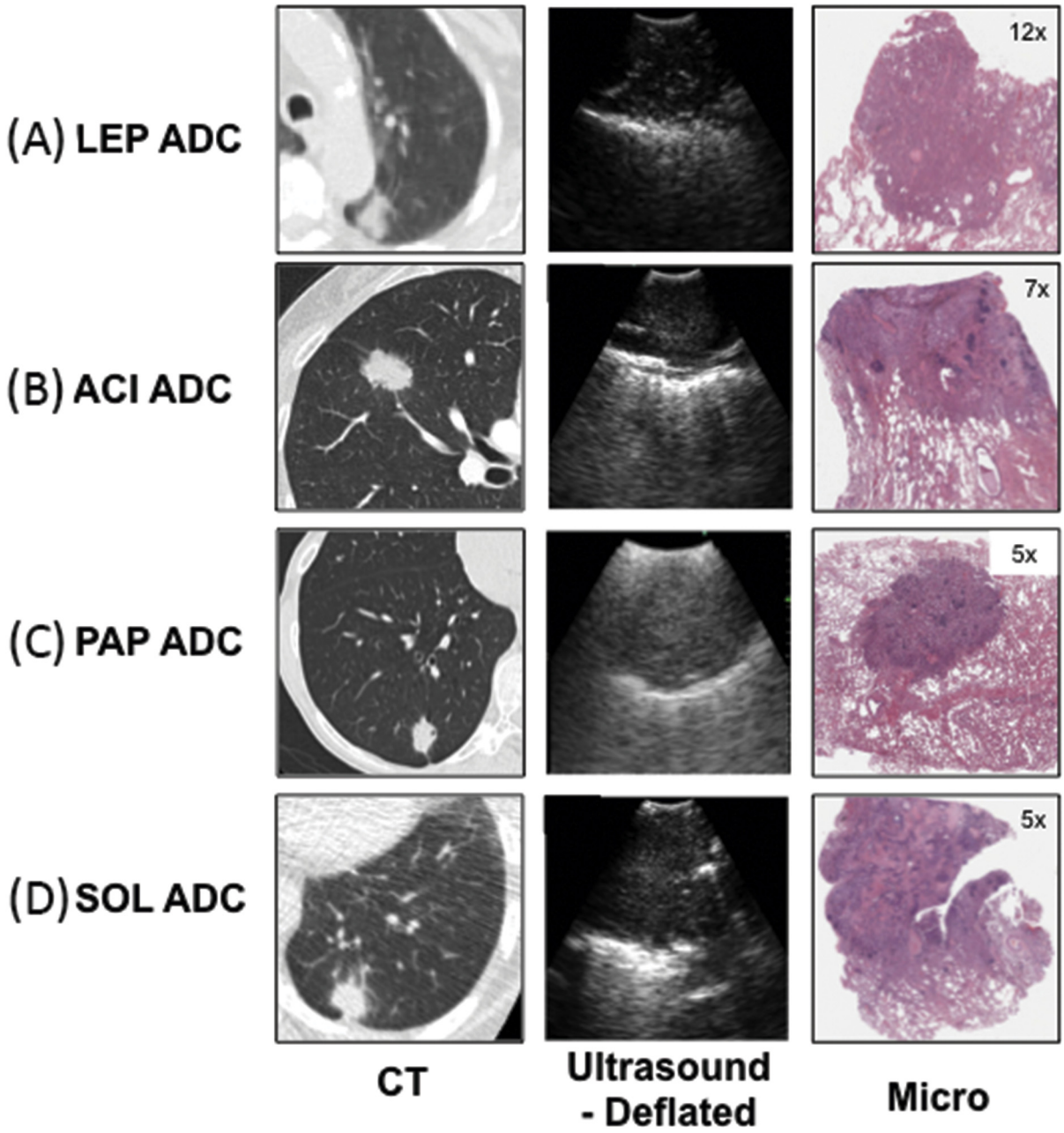

Fig 4. Comparison of lung adenocarcinoma with computed tomography (CT), ultrasound, and pathology (microscopic) images (deflated state). (Left) Computed tomography images; (middle) ultrasound images (10 MHz); (right) microscopic images (original magnification [top to bottom] ×12, ×7, ×5, and ×5). (A) Lepidic (LEP) predominant adenocarcinoma (ADC). (B) Acinar (ACI) predominant ADC. (C) Papillary (PAP) predominant ADC. (D) Solid (SOL) predominant ADC.

We acknowledge that the present device has limitations, and therefore, room for technical improvement. As shown in this study, part solid GGNs were more difficult to visualize compared with solid nodules. That may be an inherent limitation of ultrasound technology, but further investigations into the device's performance with part solid GGNs can be conducted after improvements to the device. Furthermore, in the clinical setting, the ultrasound device must be capable of localizing small and deeply seated GGNs. For this study, we had only 2 cases with tumors less than 10 mm. We will need to increase the sample size for these types of tumors to ensure the device is applicable to a wide spectrum of tumor characteristics.

In conclusion, the results of this study suggest that the ultrasound thoracoscope is capable of localizing pulmonary nodules. Tumor depth and sufficient lung deflation were found to impact the quality of the

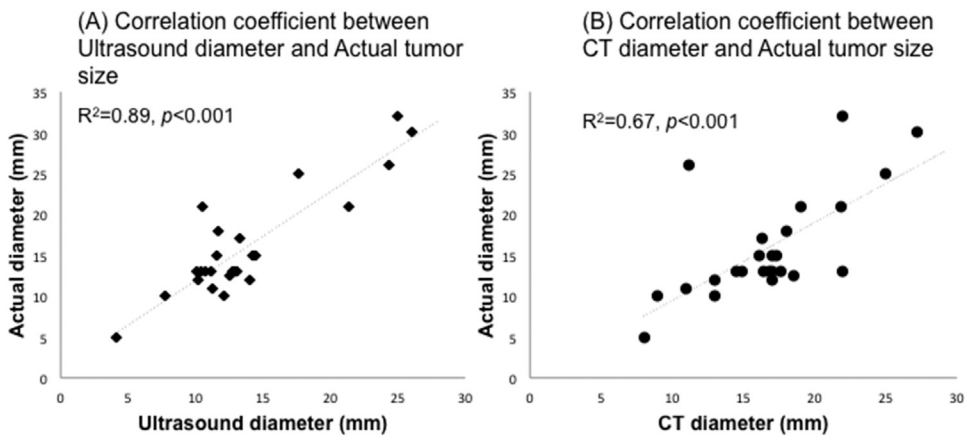

Fig 5. (A) Correlation coefficient between ultrasound diameter and actual tumor size (mm). (B) Correlation coefficient between computed tomography (CT) diameter and actual tumor size (mm). The comparison of actual distance from the lung surface to the tumor distal boundary and the distance to the distal boundary on the ultrasound image showed statistically significant and strong correlation ($R^2 = 0.89$, $p < 0.001$) compared with the actual distance from the lung surface to the tumor distal boundary and the distance to the distal boundary on the CT image ($R^2 = 0.67$, $p < 0.001$).

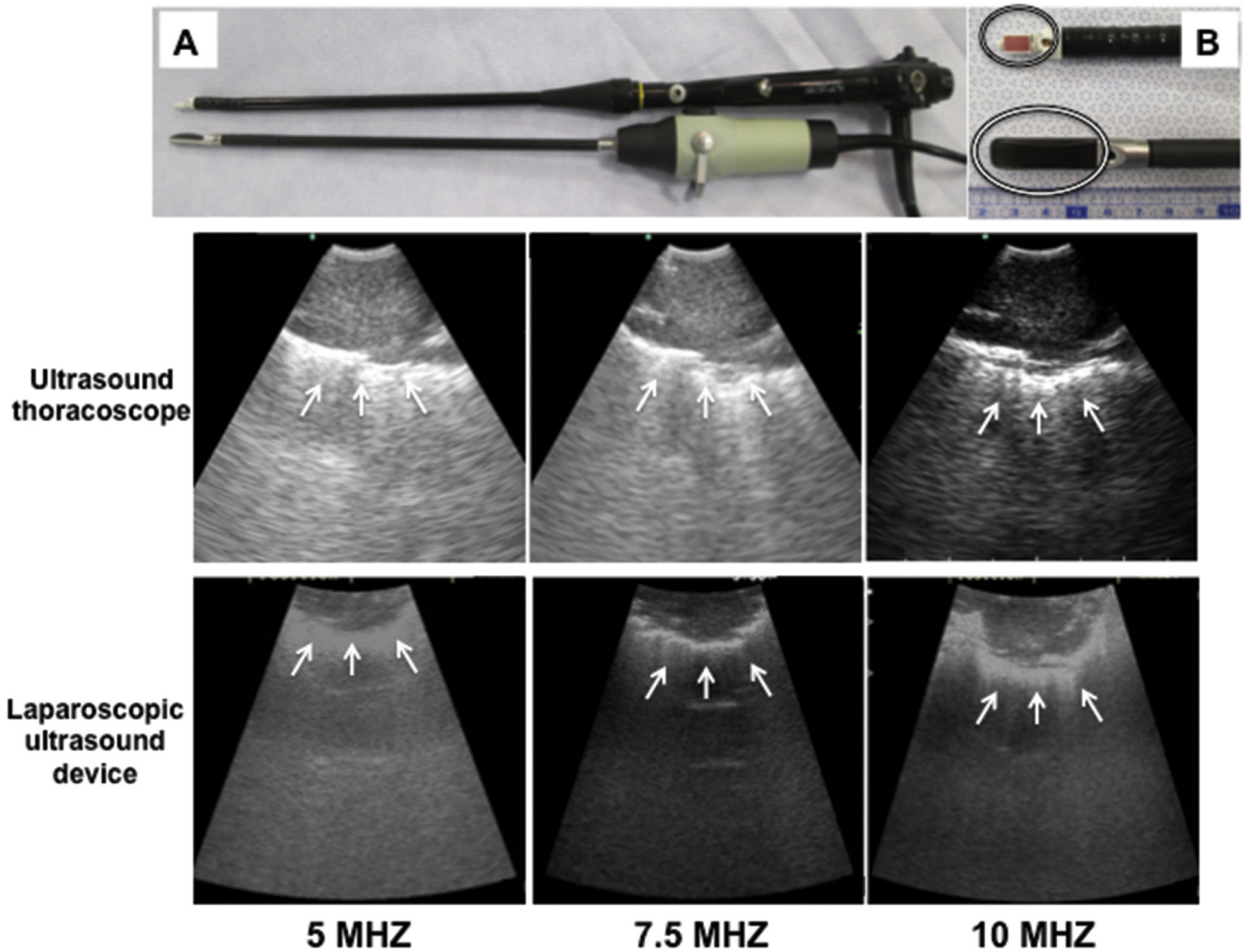

Fig 6. (A) Comparison between prototype ultrasound thoracoscope (XLTF-UC180 [top]) and laparoscopic ultrasound probe (8666-RF [bottom]). (B) Comparison of ultrasound thoracoscope probe size (top) and laparoscopic ultrasound probe size (bottom). The laparoscopic ultrasound probe is bigger than the ultrasound thoracoscope probe. (C) Comparison of image quality of ultrasound thoracoscope (top panels) and laparoscopic ultrasound (bottom panels) for a solid nodule at different frequencies: left to right, 5 MHz, 7.5 MHz, and 10 MHz. The ultrasound thoracoscope consistently produced clearer images (arrows).

ultrasound image. Moreover, ultrasound frequency also had an impact on the quality of the image produced. From 5 to 10 MHz, 10 MHz was the optimal frequency for tumor visualization. Between 10 MHz and 12 MHz, however, 12 MHz was best for visualizing shallower tumors and 10 MHz was best for visualizing deeper tumors. This study will be useful for future clinical studies of intraoperative ultrasonography.

This work was supported by the Olympus Corporation, which provided the prototype ultrasound thoracoscope (XLTF-UC180). Kazuhiro Yasufuku received research support from Olympus Corporation for conducting this study. The authors wish to thank Ms Alexandria Grindlay and Ms Judy McConnell for supporting this work.

References

1. Aberle DR, Berg CD, Black WC, et al, for the National Lung Screening Trial Research Team. The National Lung Screening Trial: overview and study design. Radiology 2011;258:243–53.
2. Mayo JR, Clifton JC, Powell TI, et al. Lung nodules: CT-guided placement of microcoils to direct video-assisted thoracoscopic surgical resection. Radiology 2009;250:576–85.
3. Kha LC, Hanneman K, Donahoe L, et al. Safety and efficacy of modified preoperative lung nodule microcoil localization without pleural marking: a pilot study. J Thoracic Imaging 2016;31:15–22.
4. Khereba M, Ferraro P, Duranceau A, et al. Thoracoscopic localization of intraparenchymal pulmonary nodules using direct intracavitary thoracoscopic ultrasonography prevents conversion of VATS procedures to thoracotomy in selected patients. J Thorac Cardiovasc Surg 2012;144:1160–5.
5. Kondo R, Yoshida K, Hamanaka K, et al. Intraoperative ultrasonographic localization of pulmonary ground-glass opacities. J Thorac Cardiovasc Surg 2009;138:837–42.
6. Gow KW, Saad DF, Koontz C, Wulkan ML. Minimally invasive thoracoscopic ultrasound for localization of pulmonary nodules in children. J Pediatr Surg 2008;43:2315–22.
7. Sortini D, Feo CV, Carcoforo P, et al. Thoracoscopic localization techniques for patients with solitary pulmonary nodule and history of malignancy. Ann Thorac Surg 2005;79:258–62.
8. Mattioli S, D'Ovidio F, Daddi N, et al. Transthoracic endosonography for the intraoperative localization of lung nodules. Ann Thorac Surg 2005;79:443–9.
9. Ambrogi MC, Dini P, Boni G, et al. A strategy for thoracoscopic resection of small pulmonary nodules. Surg Endosc 2005;19:1644–7.
10. Matsumoto S, Hirata T, Ogawa E, et al. Ultrasonographic evaluation of small nodules in the peripheral lung during video-assisted thoracic surgery (VATS). Eur J Cardiothorac Surg 2004;26:469–73.
11. Yamamoto M, Takeo M, Meguro F, Ishikawa T. Sonographic evaluation for peripheral pulmonary nodules during video-assisted thoracoscopic surgery. Surg Endosc 2003;17:825–7.
12. Piolanti M, Coppola F, Papa S, Pilotti V, Mattioli S, Gavelli G. Ultrasonographic localization of occult pulmonary nodules during video-assisted thoracic surgery. Eur Radiol 2003;13:2358–64.
13. Wada H, Anayama T, Hirohashi K, et al. Thoracoscopic ultrasonography for localization of subcentimetre lung nodules. Eur J Cardiothorac Surg 2016;49:690–7.
14. Travis WD, Brambilla E, Konrad Müller-Hermelink H, Harris CC, eds. WHO classification of tumours of the lung, pleura, thymus and heart. Vol 7. 4th ed. Geneva, Switzerland: WHO Press, 2015.
15. Ujiie H, Kadota K, Chaft JE, et al. Solid predominant histologic subtype in resected stage I lung adenocarcinoma is an independent predictor of early, extrathoracic, multisite recurrence and of poor postrecurrence survival. J Clin Oncol 2015;33:2877–84.